Oxygen 1s x-ray-absorption near-edge structure of Zn-Ni ferrites: A comparison with the theoretical calculations

W. F. Pong and M. H. Su

Department of Physics, Tamkang University, Tamsui, Taiwan 251, Republic of China

M.-H. Tsai

Department of Physics, National Sun Yat-Sen University, Kaohsiung, Taiwan 804, Republic of China

H. H. Hsieh, J. Y. Pieh, Y. K. Chang, K. C. Kuo, and P. K. Tseng

Department of Physics, Tamkang University, Tamsui, Taiwan 251, Republic of China

J. F. Lee, S. C. Chung, C. I. Chen, K. L. Tsang, and C. T. Chen

Synchrotron Radiation Research Center (SRRC), Hsinchu Science-based Industrial Park, Taiwan 300, Republic of China

(Received 26 June 1996)

We present the electronic structure of ferrimagnetic $Zn_xNi_{1-x}Fe_2O_4$ compounds obtained by a combination of O K-edge x-ray-absorption measurements and first-principles spin-unrestricted calculations using the pseudofunction method. The two distinct preedge features are found to vary systematically as a function of the Zn content. From both experimental and theoretical analyses, we find that substitution of Ni with Zn enhances localization of the $3d$ states of Fe on the octahedral sites, so that the O $2p$–Fe $3d$ hybridized states can be resolved into two distinct twofold and threefold features. [S0163-1829(96)01147-2]

I. INTRODUCTION

Ferrimagnetic spinel $Zn_xNi_{1-x}Fe_2O_4$ compounds have been of fundamental and practical interests over the past years. Mössbauer studies,[1,2] based on the existence of two hyperfine fields, have suggested that the structures of Zn-Ni ferrites contain two distinct sites, namely, the tetrahedral and octahedral sites. Site-preference calculations[3] and neutron-diffraction studies[4] proposed that Zn^{2+} ions have a strong tendency to occupy the tetrahedral A sites (A). On the other hand, the Ni^{2+} ions are excluded from occupying the A sites, and are believed to be on the octahedral B sites (B). The cation distribution in the Zn-Ni ferrites can be expressed quantitatively by $(Zn_xFe_{1-x})_A(Ni_{1-x}Fe_{1+x})_BO_4$, where the metallic cations are enclosed by $()_A$ and $()_B$, respectively, for occupying A and B sites. In $Zn_xNi_{1-x}Fe_2O_4$ compounds the metallic cations occupying the A and B sites are surrounded by four and six nearest-neighbor (NN) oxygen anions, respectively.

Band-structure calculations based on the local spin-density-functional theory for two extreme cases of $ZnFe_2O_4$ ($x=1$) and $NiFe_2O_4$ ($x=0$) have been reported previously.[5] However, the electronic structures of $Zn_xNi_{1-x}Fe_2O_4$ for $0<x<1$ are still unknown. A combination of the O K-edge x-ray-absorption near-edge structure (XANES) measurements and first-principles spin-unrestricted calculations enable us not only to obtain the electronic structures but also to gain insight into the couplings between metallic $3d$ states and oxygen $2p$ states. We are particularly interested in their dependence on Zn substitution of Ni in these compounds.

II. EXPERIMENTS

The O K-edge XANES measurements of $Zn_xNi_{1-x}Fe_2O_4$ ($x=0.0$, 0.13, 0.25, 0.38, 0.50, 0.63, 0.75, 0.88, and 1.0)

were performed at the high-energy spherical grating mono-chromator beamline, with an electron beam energy of 1.3 GeV and a maximum stored current of 200 mA, at the Synchrotron Radiation Research Center in Hsinchu, Taiwan. For these machine units, the energy resolution of the monochro-mator at the energy range of interest, ~550 eV, was set at ~0.5 eV. The absorption spectra were obtained by collecting the soft-x-ray fluorescence yield with a high-sensitivity seven-element germanium detector. The energy scale was calibrated using the well-known spectrum of a CaF_2 thin film. In this study, $Zn_xNi_{1-x}Fe_2O_4$ compounds were prepared with the usual ceramic method; the details of the sample preparations have been described elsewhere.[6] The samples were characterized with x-ray diffraction and energy-dispersive x-ray fluorescence analysis, then pressed into pellets and placed in the ultrahigh-vacuum system. All measurements were performed at room temperature.

III. THEORY

The first-principles spin-unrestricted pseudofunction (PSF) method[7] was employed to calculate systematically the projected density of states (DOS) of the $ZnFe_2O_4$, $Zn_{0.5}Ni_{0.5}Fe_2O_4$, and $NiFe_2O_4$ compounds. This method has been shown to work well for the magnetic properties of transition metals.[7] The local spin-density approximation is employed in the form of the von Barth–Hedin exchange-correlation functional.[8] Scalar-relativistic effects are included for all metals. The potential is divided into spheri-cal potentials within the muffin-tin spheres, and a nonspheri-cal potential that extends throughout the crystal and is expanded in the plane waves. PSF's are smooth mathematical functions constructed to match the muffin-tin-orbitals tails continuously and differentially outside the muffin-tin
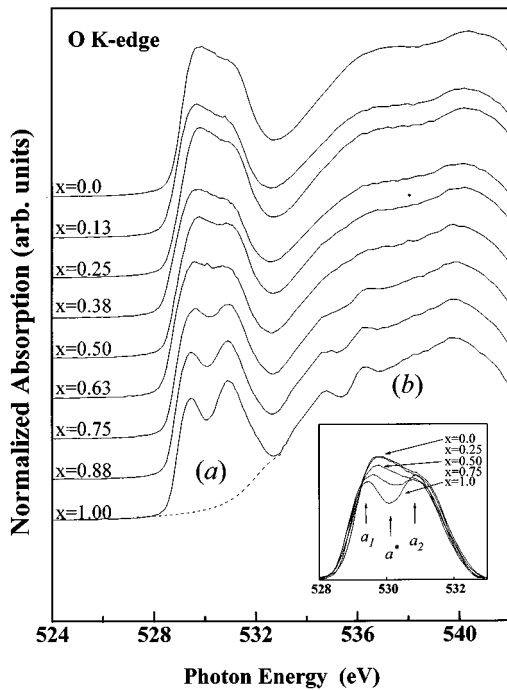
FIG. 1. Normalized fluorescence yield at the O K-edge absorption spectra of $Zn_xNi_{1-x}Fe_2O_4$. The dashed line is a best-fitted Gaussian shape background. The region of feature a after the background subtraction is inset on a magnified scale.

spheres. They are simply devised to calculate the interstitial parts of matrix elements efficiently.[7] We expand PSF's in 12 167 ($23 \times 23 \times 23$) plane waves. Nonspherical parts of the charge density and potential are expanded in 91 125 ($45 \times 45 \times 45$) plane waves. We use a single special point to obtain the self-consistent charge density and potential and then use ten special **k** points for a face-centered-cubic Bravais lattice[9] to obtain the projected DOS. $ZnFe_2O_4$, $Zn_{0.5}Ni_{0.5}Fe_2O_4$, and $NiFe_2O_4$ have a spinel structure with lattice constants 15.779, 15.866, and 15.953 a.u., respectively.[1] The unit-cell parameters and atomic positions are determined from the x-ray crystallography table.[10] Muffin-tin radii of 2.21, 2.23, 2.25, and 1.2 a.u. are chosen for Fe, Ni, Zn, and O, respectively, which are roughly proportional to their covalent radii[11] with the constraint that all muffin-tin spheres do not overlap.

IV. RESULTS AND DISCUSSION

Figure 1 shows the O K-edge fluorescence yield XANES spectra of $Zn_xNi_{1-x}Fe_2O_4$. The spectra are normalized to have the same area in the energy range between 550 and 570 eV (not fully shown in the figure). According to the dipole-transition selection rules, the O K-edge XANES spectra reflect transitions to oxygen unoccupied $2p$-derived states, which have been hybridized with the relatively narrow $3d$ and broader $4sp$ bands of the $3d$-transition-metal above the Fermi level, which result in features a and b on the spectra, respectively. To understand feature a, we analyze the couplings between O $2p$ and transition-metal $3d$ states for various Zn substitutions in $Zn_xNi_{1-x}Fe_2O_4$. The inset of Fig. 1 shows the spectra of feature a for several Zn concentrations after subtraction of the background. (The background intensity in Fig. 1 was subtracted by using a best-fitted Gaussian
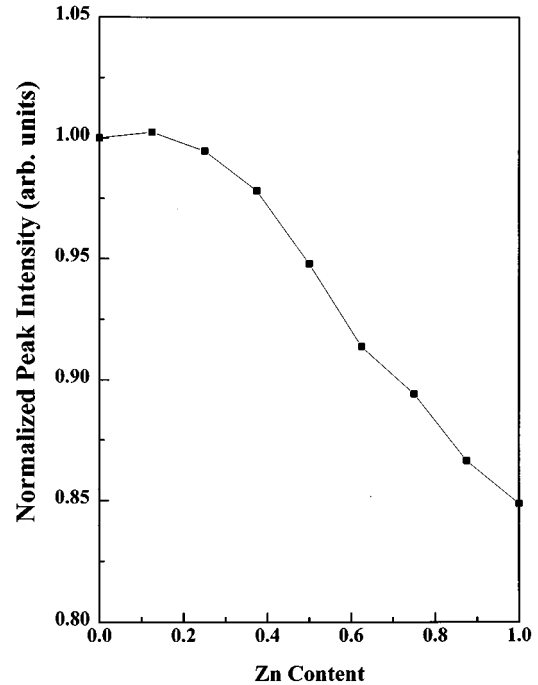

FIG. 2. The integrated intensity of feature a at the O K-edge as a function of x for $Zn_xNi_{1-x}Fe_2O_4$ normalized to that of $NiFe_2O_4$.

line shape as shown by the dashed-line curve.) It exhibits two-peak features a_1 and a_2 above the threshold, located at 529.5 and 531.0 eV, respectively. They are best resolved for $ZnFe_2O_4$ ($x=1$), and are least resolved for $NiFe_2O_4$ ($x=0$). a_1 shifts slightly toward higher energy with decreasing x. There is an additional feature a^* located between peaks a_1
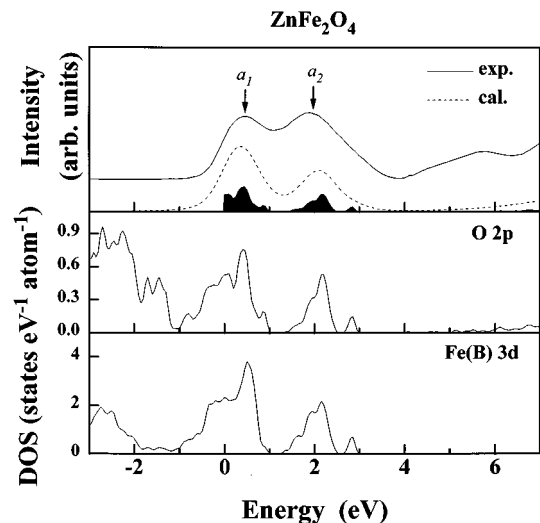

FIG. 3. Comparison of the O K-edge x-ray-absorption feature a (upper solid line) with a convolution of the theoretical oxygen p-projected DOS with the core-hole lifetime and instrumental broadening (upper dashed line) for $ZnFe_2O_4$. The spectra have been aligned at the position of the first peak, and the intensity units have been normalized arbitrarily. The darkened area is the theoretical oxygen p-projected DOS above the Fermi level, which is defined as the zero energy.
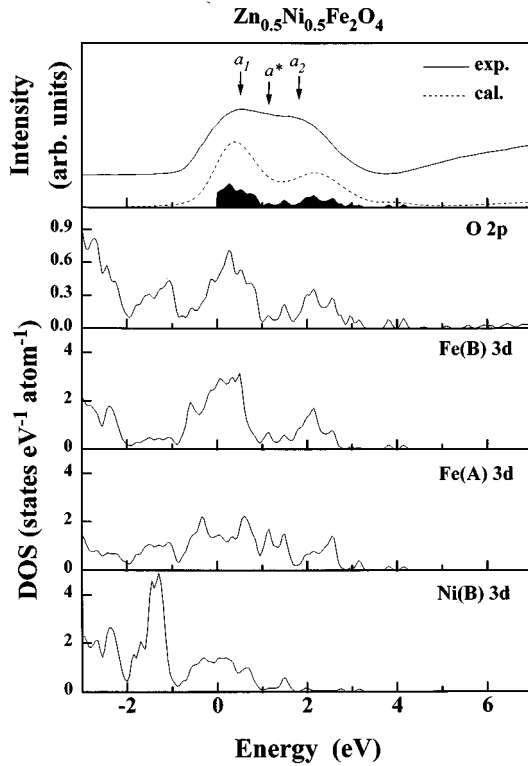
FIG. 4. Comparison of the O K-edge x-ray-absorption feature a (upper solid line) with a convolution of the theoretical oxygen p-projected DOS with the core-hole lifetime and instrumental broadening (upper dashed line) for $Zn_{0.5}Ni_{0.5}Fe_2O_4$.
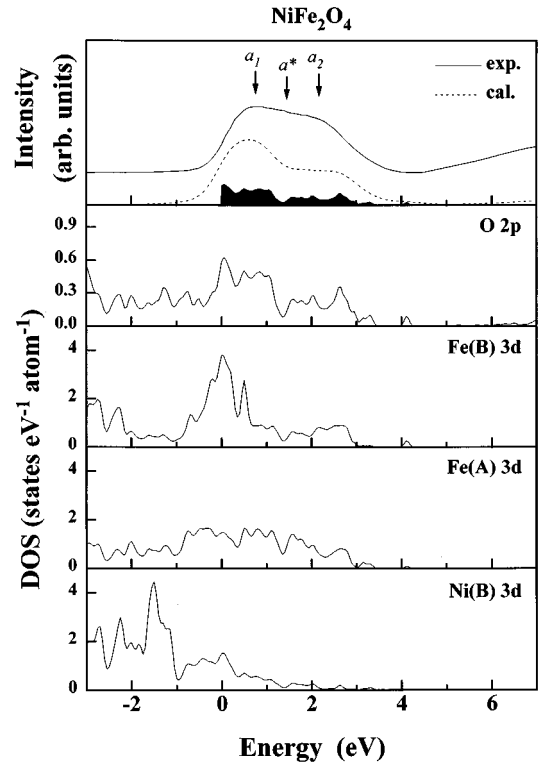
FIG. 5. Comparison of the O K-edge x-ray-absorption feature a (upper solid line) with a convolution of the theoretical oxygen p-projected DOS with the core-hole lifetime and instrumental broadening (upper dashed line) for $NiFe_2O_4$.

and a_2; its intensity decreases with the increase of x. Similar two-peak features at the threshold of the O K edge were obtained in the $3d$-transition-metal oxides.[12,13] We have integrated the intensity of feature a between 528 and 533 eV, and plotted our results as a function of x in Fig. 2 to see the overall effect of Zn substitution. When x is increased from zero, the intensity of feature a remains more or less constant up to $x=0.25$, beyond which it decreases, as shown in Fig. 2. The decrease of the intensity of feature a with the increase x indicates that Zn substitution reduces couplings of the O $2p$ orbitals with metallic $3d$ orbitals. This happens because Zn $3d$ energy levels are situated further away in energy from the O $2p$ states than the Fe and Ni $3d$ states in these compounds, so that Zn makes an insignificant contribution to O $2p$ metallic $3d$ couplings. This is in agreement with a generally accepted rule that hybridization effects in transition-metal oxides are smaller in the late-transition-metal than in the early-transition-metal oxides.[12] Thus Zn substitution reduces the number of available metallic $3d$ states that can couple to O $2p$ states, and causes a decrease in the intensity of feature a with the increase of x.

In Figs. 3, 4, and 5, we compare O K-edge XANES spectra and calculated oxygen p-projected DOS's for $ZnFe_2O_4$, $Zn_{0.5}Ni_{0.5}Fe_2O_4$, and $NiFe_2O_4$, respectively. The lower darkened area shows the theoretical oxygen p-projected DOS above the Fermi level. The upper solid curve is an O K-edge absorption spectra of feature a, and the dashed curve in the middle is the theoretical oxygen p-projected DOS broadened with a Lorentzian of 0.3 eV to simulate the core-hole lifetime,[14] and convoluted with a Gaussian function of 0.5

eV to simulate the experimental resolution. The calculated electronic structures for these three samples ($x=1.0$, 0.5, and 0.0) differ significantly for the $3d$ states of Fe(A), Fe(B), and Ni(B), as shown in Figs. 3, 4, and 5. The Fe(B) $3d$ states spread widely up to about 3 eV above the Fermi level. They are split into two-peak features when the Zn concentration is increased up to $x=1$ ($ZnFe_2O_4$). In contrast, the Fe(A) $3d$ states, are relatively insensitive to the change of the Zn content, except that the $3d$ band is more or less broadened for $x\rightarrow 0$. The Ni(B) $3d$ states have a relatively smaller DOS above the threshold region in comparison with those of Fe(A) and Fe(B). Our theoretical calculations are also in agreement with earlier published studies,[5] showing that the two distinct peaks a_1 and a_2 in $ZnFe_2O_4$ observed at photon energies around 0.5 and 2.0 eV, as shown in Fig. 3, are due to O $2p$–Fe(B) $3d$ hybridization with t_{2g} and e_g symmetries, respectively. The energy difference between these two states, referred to as the ligand-field parameter $10Dq\approx 1.5$ eV, is comparable with that of the iron oxides reported in the earlier literature.[12] In contrast to the two-peak features observed for $ZnFe_2O_4$ more complicated spectra exhibiting some multiplet structures were observed for $Zn_{0.5}Ni_{0.5}Fe_2O_4$ and $NiFe_2O_4$. The corresponding features a_1 and a_2 shown in Figs. 4 and 5 are primarily contributed by O $2p$–Fe(B) $3d$ and O $2p$–Fe(A) $3d$ hybridized states with a relatively smaller contribution by the Ni(B) $3d$ states. a_1 has previously been observed to shift slightly toward higher energy with decreasing Zn content in $Zn_x Ni_{1-x}Fe_2O_4$, in agreement with present observations. Feature a^* is primarily
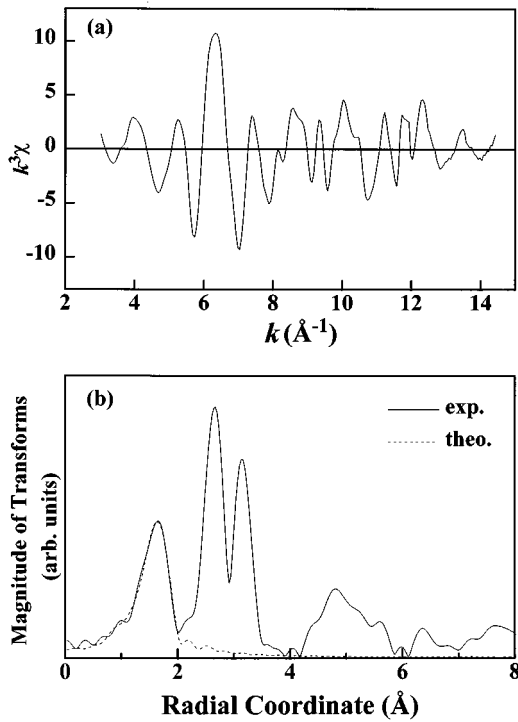
FIG. 6. (a) Normalized Fe K-edge EXAFS oscillations $\chi(k)$ weighted by k^3 for $Zn_{0.5}Ni_{0.5}Fe_2O_4$ at room temperature. (b) Magnitude of the Fourier transform of the EXAFS $k^3\chi$ data from $k=3.5$ to 13.5 Å^{-1} (solid line). Final fit of theory to the nearest-neighbor Fe(A)-O and Fe(B)-O bond lengths (dashed line). Structural parameters of two nearest neighbors obtained by fitting the Fe K-edge EXAFS spectrum: $N_{Fe(A)-O}=4$, $R_{Fe(A)-O}=1.92\pm0.01$ Å, $\sigma^2_{Fe(A)-O} = (4.8\pm1.2)\times10^{-3}$ Å^2, $N_{Fe(B)-O}=6$, $R_{Fe(B)-O}=2.01\pm0.01$ Å, and $\sigma^2_{Fe(B)-O}=(5.3\pm1.0)\times10^{-3}$ Å^2. N is the coordination number, R the nearest-neighbor distance, and σ^2 the mean-square vibrational amplitude.

contributed by the Fe(A) $3d$, states with a smaller contribution by Fe(B) $3d$ states.

It is generally believed that different p-d hybridization effects in transition-metal compounds can be explained by energy separations between the transition-metal $3d$ and anion p states as well as NN transition-metal–anion bond lengths.[15] Harrison showed that the square of the hybridization coupling constant, V^2_{pd}, is proportional to (r^3_d/d^7),[16] where r_d and d are the transition-metal d-orbital radius and the NN transition–metal-oxygen bond lengths, respectively. r_d's are 0.80 and 0.72 Å for Fe and Ni,[16] respectively. The extended x-ray-absorption fine structure (EXAFS) was performed at the Fe and Ni K edge in $Zn_xNi_{1-x}Fe_2O_4$ using transmission mode measurements at room temperature.[17] The normalized EXAFS oscillations $\chi(k)$ are weighted by k^3 for both Fe and Ni K edges, and the corresponding Fourier transforms of the $k^3\chi$ data for $Zn_{0.5}Ni_{0.5}Fe_2O_4$ are shown in Figs. 6 and 7, respectively. Our analysis involved the use of a combination of the multiple-scattering EXAFS computer program FEFF5,[18] and the nonlinear least-squares-fitting computer program FEFFIT.[19] As shown in Figs. 6(b) and 7(b), the quality of the fit for the NN Fe(A)-O, Fe (B)-O, and Ni(B)-O bond lengths in Figs. 6(b) and 7(b) are quite good. We obtained NN bond lengths of $\sim1.92\pm0.02$ Å, ~2.00

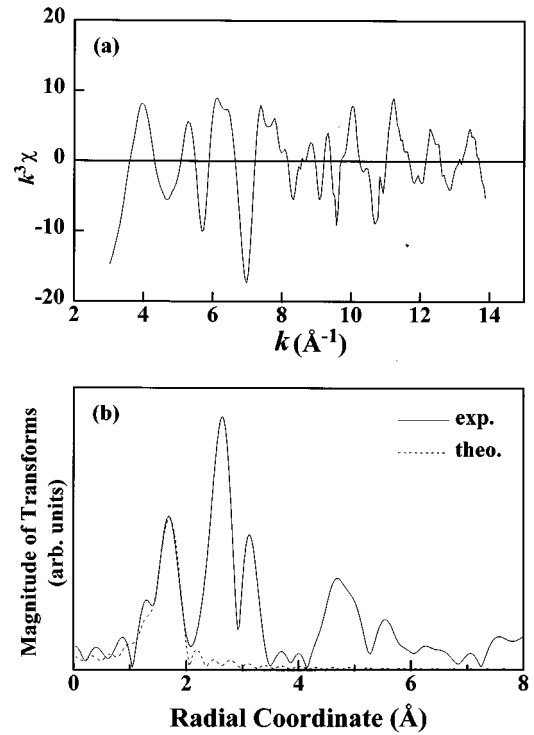FIG. 7. (a) Normalized Ni K-edge EXAFS oscillations $\chi(k)$ weighted by k^3 for $Zn_{0.5}Ni_{0.5}Fe_2O_4$ at room temperature. (b) Magnitude of the Fourier transform of the EXAFS $k^3\chi$ data from $k=3.5$ to 13.9 Å^{-1} (solid line). Final fit of theory to the nearest-neighbor Ni(B)-O bond lengths (dashed line). Structural parameters of the nearest neighbor obtained by fitting the Ni K-edge EXAFS spectrum: $N_{Ni(B)-O}=6$, $R_{Ni(B)-O}=2.06\pm0.01$ Å, and $\sigma^2_{Ni(B)-O}=(5.9\pm2.5)\times10^{-3}$ Å^2. N is the coordination number, R the nearest-neighbor distance, and σ^2 the mean-square vibrational amplitude.

±0.02 Å, and $\sim2.06\pm0.02$ Å for Fe(A)-O, Fe(B)-O, and Ni(B)-O, respectively, throughout the series of $Zn_xNi_{1-x}Fe_2O_4$. Harrison's formula yields that V_{pd} increases in the order Ni(B)-O, Fe(B)-O and Fe(A)-O, since Fe has a smaller atomic number than Ni in the $3d$-transition-metal series, and Fe(A)-O has the shortest NN bond length. Thus Fe(A) $3d$ states have a higher hybridization probability with the O $2p$ states than Fe(B) and Ni(B) $3d$ states, especially for smaller Zn substitution for $Zn_xNi_{1-x}Fe_2O_4$. In addition, since Zn ions occupy the A sites while Ni ions occupy the B sites, the decrease of the Zn content means the increase of the Ni content and a movement of Fe^{3+} ions from the B sites to the A sites. In other words, the decrease of x means the increase of the number of Fe(A) ions, and further enhances the O $2p$–Fe(A) $3d$ couplings. This implies that feature a^* is related to the increase of the width of O $2p$–Fe(A) $3d$-hybridized states with the decrease of Zn substitution in the A sublattice, which agrees with our theoretical calculations as shown in Figs. 4 and 5.

Finally, feature b (occurring between 533 and 542 eV) in the spectrum of Fig. 1 is significantly broader than feature a, and contains some weakly oscillating structures in the region between ~534 and 537 eV. Its line shape becomes sharper with increasing x for $x\geqslant0.75$. We suspect that these weak structures may be related to the unoccupied O $2p$–Zn $4sp$ hybridized states.[20]

V. CONCLUSIONS

From our results of O K-edge XANES spectra and first-principles spin-unrestricted calculations, we found that the two distinct preedge features vary systematically as functions of the Zn content in $Zn_xNi_{1-x}Fe_2O_4$. Peaks a_1 and a_2 are dominantly contributed by the O $2p$–Fe(B) $3d$- and O $2p$–Fe(A) $3d$-hybridized states corresponding to the t_{2g} and e_g $3d$ subbands, respectively. On the other hand, feature a^* is strongly related to Fe(A) $3d$ states because Fe(A) $3d$ states have a higher hybridization probability with the O $2p$ states than Fe(B) and Ni(B) $3d$ states in $Zn_xNi_{1-x}Fe_2O_4$.

[1] L. K. Leung, B. J. Evans, and A. H. Morrish, Phys. Rev. B **8**, 29 (1973).
[2] S. C. Bhargava and N. Zeman, Phys. Rev. B **21**, 1717 (1980).
[3] J. Smit and H. P. J. Wijn, *Ferrites* (Wiley Interscience, New York, 1959).
[4] N. S. Satya Murthy, M. G. Natera, S. I. Youssef, R. J. Begum, and C. M. Srivastava, Phys. Rev. **181**, 969 (1969).
[5] M. Pénicaud, B. Siberchicot, C. B. Sommers, and J. Kübler, J. Magn. Magn. Mater. **103**, 212 (1992).
[6] T. M. Uen and P. K. Tseng, Phys. Rev. B **25**, 1848 (1982).
[7] R. V. Kasowski, M.-H. Tsai, T. N. Rhodin, and D. D. Chambliss, Phys. Rev. B **34**, 2656 (1986); M.-H. Tsai and K. C. Hass, *ibid*. **51**, 14 616 (1995); K. C. Hass, M.-H. Tsai, and R. V. Kasowski, *ibid*. **53**, 44 (1996).
[8] U. von Barth and L. Hedin, J. Phys. C **5**, 1629 (1972).
[9] D. J. Chadi and M. L. Cohen, Phys. Rev. B **8**, 5747 (1973).
[10] *International Tables for X-ray Crystallography*, edited by N. F. M. Henry and K. Lonsdale (Kynoch, Birmingham, 1969), Vol. 1.
[11] *Table of Periodic Properties of the Elements* (Sargent-Welch Scientific Company, Skokie, IL, 1980).
[12] F. M. F. deGroot, M. Grioni, J. C. Fuggle, J. Ghijsen, G. A. Sawatzky, and H. Petersen, Phys. Rev. B **40**, 5715 (1989).
[13] H. Kurata, E. Lefevre, C. Colliex, and R. Brydson, Phys. Rev. B **47**, 13 763 (1993).
[14] F. M. F. de Groot, J. C. Fuggle, and J. M. van Ruitenbeek, Phys. Rev. B **44**, 5280 (1991).
[15] B. E. Larson, K. C. Hass, H. Ehrenreich, and A. E. Carlsson, Phys. Rev. B **37**, 4137 (1988).
[16] W. A. Harrison, *Electronic Structure and the Properties of Solids* (Freeman, San Francisco, 1980).
[17] W. F. Pong *et al.* (unpublished).
[18] J. M. de Leon, Y. Yacoby, E. A. Stern, and J. J. Rehr, Phys. Rev. B **42**, 10 843 (1990); J. J. Rehr, J. M. de Leon, S. I. Zabinsky, and R. C. Albers, J. Am. Chem. Soc. **113**, 5135 (1991).
[19] A. I. Frenkel, E. A. Stern, M. Qian, and M. Newville, Phys. Rev. B **48**, 12 449 (1993).
[20] D. A. Papaconstantopoulos, *Handbook of the Band Structure of Elemental Solids* (Plenum, New York, 1986).